AIRCRAFT WING STRUCTURE MONITORING USING AN INTEGRATED IMPEDANCE AND GUIDED WAVE TECHNIQUE

Y.K. An[1]*, H. Sohn[1] , C.Y. Park[2]
[1] Department of Civil and Environmental Engineering, KAIST, Daejeon, 305-701, Korea
[2] Agency for Defense Development, Daejeon, 305-600, Korea
* Corresponding author (ayk2028@kaist.ac.kr)

Keywords: *Structural Health Monitoring, Aircraft Wing Structure, Full Scale Test, Integrated Impedance and Guided Wave Technique*

1. Introduction

Recently, aircraft monitoring has attracted tremendous interest to many researchers in the field of structural health monitoring (SHM) and nondestructive testing (NDT). For example, guided wave and impedance based SHM techniques using surface-mounted piezoelectric transducers (PZTs) have been widely used for detecting hidden damages in aircraft structures due to their sensitivity to small structural changes [1-4]. Guided wave and impedance based techniques have their own merits for local damage detection, because they identify damage based on different physical principles.
In this study, a robust damage detection system is developed and validated through full scale tests for an aircraft wing segment. First, impedance and guided wave data acquisition system that can simultaneously obtain the two data is developed. Then an integrated impedance and guided wave (IIG) based damage detection technique is developed to enhance the performance and reliability of damage diagnosis under environmental variation. Finally, the applicability of the proposed technique to full scale aircraft wing structure is investigated under varying temperature and loading conditions. From design step for the test structure, structural hot spots are selected through structural analysis, and the necessary sensors are embedded. Two types of actual hidden damage in upper skin and a fitting lug are investigated in this study.

2. Theoretical Development

The admittance response (Y), the inverse of the impedance (1/Y) in an electro-mechanical system composed of a host structure and a PZT can be expressed as follows [5].

$$\overline{Y} = \omega j \frac{\omega_a l_a}{h_a}\left[\bar{\varepsilon}_{33}^{T} + \left(\frac{z_a}{z_a + z}\right) d_{31}^2 \overline{Y}_{11}^{E}\left(\frac{\tan \kappa l_a}{\kappa l_a}\right) - d_{31}^2 \overline{Y}_{11}^{E}\right] \quad (1)$$

where l_a , ω_a and h_a indicate the length, width, and thickness of the PZT, respectively. d_{31} is the piezoelectric strain coefficient and $\bar{\varepsilon}_{33}^{T} = \varepsilon_{33}^{T}(1-\delta j)$ is the complex electric permittivity of the PZT material at constant stress. $\overline{Y}_{11}^{E} = Y_{11}^{E}(1+\eta j)$ is the complex Young's modulus of PZT material at constant electric field. Here, δ and η denote the dielectric loss factor and mechanical loss factor of the PZT. ω , κ , z_a , and z represent the angular frequency, wave number, mechanical impedance of the PZT, and short-circuited mechanical impedance of the host structure, respectively. The admittance signal can be decomposed into active and passive components as follow [6].

$$\overline{Y} = \overline{Y}_P + \overline{Y}_A \quad (2)$$

where $\overline{Y}_P = \omega j \frac{\omega_a l_a}{h_a}\left[\bar{\varepsilon}_{33}^{T} - d_{31}^2 \overline{Y}_{11}^{E}\right]$

and $\overline{Y}_A = \omega j \frac{\omega_a l_a}{h_a}\left(\frac{z_a}{z_a + z}\right) d_{31}^2 \overline{Y}_{11}^{E}\left(\frac{\tan \kappa l_a}{\kappa l_a}\right)$

$\overline{Y}_P$ is the passive admittance depending on only the PZT parameters, and $\overline{Y}_A$ is called the active admittance including the mechanical impedance as well as the PZT impedance term [6]. Since $\overline{Y}_P$ is not affected by the change of the host structure's mechanical properties, it is used for the environmental effect compensation. Subsequently, the corresponding $\overline{Y}_A$ and guided waves (G) are used for damage detection.
The IIG based damage detection algorithm starts with the collection of admittance and guided wave data sets from the baseline and test conditions of the structure. Then, the measured admittance signals are decomposed into active and passive components using Eq. (2). Once the passive admittance signal obtained from a damage-suspected target structure is extracted, the two closest passive

admittance signals obtained from the collected baseline data can be selected.

Next, damage indices, DI_A for the active admittance and DI_G for the guided wave, are respectively calculated using a cross-correlation coefficient between the test data set and the closest baseline data set [7]. The final damage index (DI) for damage diagnosis is computed from the weighted summation of DI_A and DI_G. Then, threshold values, TR_A for the active admittance and TR_G for the guided wave, are similarly computed using the cross-correlation coefficient between the two selected baseline data sets. The final threshold (TR) is obtained through the same procedure as DI. Based on the DI and TR values, damage diagnosis can be simply performed as following statement.

"If DI *is smaller than* TR, *damage is alarmed. Otherwise, no alarm is triggered".*

This algorithm is carried out based on the premise that the correlation between the test data and the closest baseline data should be higher than the correlation between two selected baseline data sets unless the test data set is measured from a damaged structure.

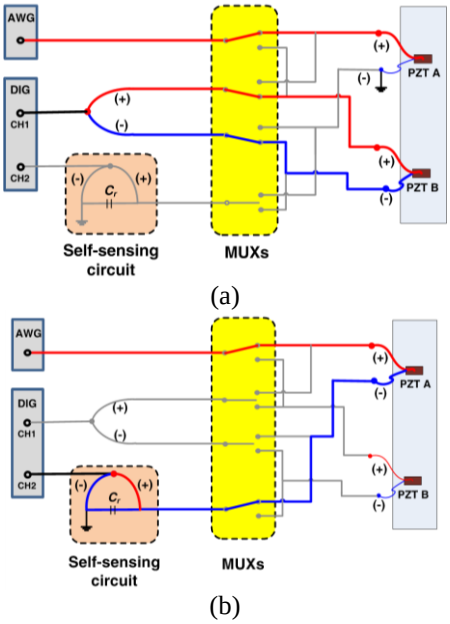

Fig. 1 Circuit design of the IIG measurement system: (a) pitch-catch mode for guided wave measurement and (b) pulse-echo mode for admittance measurement. Note that the darker lines denote the activated lines.

3. Development of an IIG Measurement System

An IIG measurement system is developed so that impedance and guided wave data can be obtained via a single hardware system. Since different data acquisition systems can cause enormous operational error, the use of a single data acquisition system is necessarily required. The developed hardware system consists of a 16-bits arbitrary waveform generator (AWG), a two channel 14-bits high-speed digitizer (DIG) and two multiplexers (MUXs) with a 500 MHz switching speed. The high-speed MUXs are used for collecting data in two different modes as shown in Fig. 1. Fig. 1(a) allows us to create guided waves using AWG at PZT A and measure the corresponding responses using DIG at PZT B. Fig. 1(b) make it possible to measure the admittance at PZT A. Here, a self-sensing circuit is inserted between the PZT and DIG so that admittance of the PZT can be obtained [8]. Although the two-channel data acquisition system is shown in Fig. 1, we can easily extend it to multi-channel data acquisition system by employing more high-speed multiplexers.

4. Full Scale Test

The applicability of the proposed technique is examined in a full scale aircraft wing structure. Fig. 2 shows a full scale composite aircraft wing structure. The structure consisted of a carbon fiber reinforced composite wing and two aluminum fitting lugs, and it is fixed on the specially manufactured jig as displayed in Fig. 2. Here, two hydraulic actuators and a displacement sensor were employed for external loading tests.

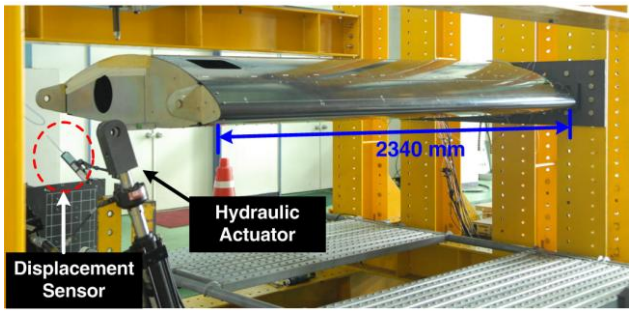

Fig. 2 A full scale composite aircraft wing segment and hydraulic actuators and a displacement sensor used for external loading tests

The PZT installations and artificially introduced actual damages are displayed in Fig. 3. The possible two damage types, debonding between the upper skin and a stringer, and bolt loosening at a main fitting lug, were determined from the structural design step through structural analysis.

Three identical PZTs with 0.508 mm and the diameter of 20 mm were placed among stringers on the inner surface of the upper skin. 10 mm-debonding was artificially introduced between the upper skin and a stringer as shown in Fig. 3 (a). For fitting lug, a PZT with 3 mm and the diameter of 30 mm were installed. The marked bolt shown in Fig. 3 (b) was loosened by 360° turn.

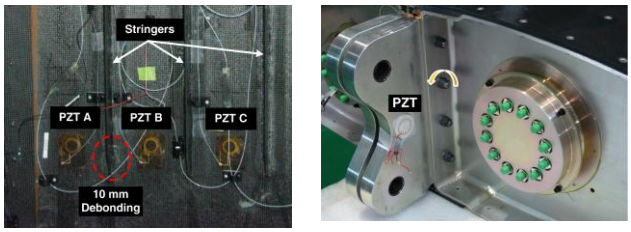

(a) (b)

Fig. 3. PZT installations and introduced actual damages: (a) Three identical PZTs were placed among stringers on the inner surface of upper skin. 10 mm-debonding was introduced between the upper skin and a stringer. (b) A PZT was placed at a fitting lug. The marked bolt was loosened by 360° turn.

The baseline data sets were collected from the intact condition of the structure at 20℃, 28℃, 34℃, and 40℃ under self-weighting condition, and they also were collected from the intact structure at 20℃ under up and down bending of 1.3kN, 3.9kN and 6.5kN using the hydraulic actuators. Here, the critical spots of interest were locally heated for temperature variation tests, because it is hard to intentionally heat up the whole target structure due to its large size. Subsequently, the test data sets were obtained from the intact and damaged conditions at 22℃ under self-weighting condition. The test data sets obtained from the intact condition were used for false-positive testing, and the damaged data sets for false-negative testing.

Fig. 4 shows the changes of both admittance and guided wave signals obtained from the upper skin of the aircraft wing structure due to temperature variation. Here, the admittance signals were generated and measured at PZT A installed on the intact target structure as shown in Fig. 3 (a). Then the guided waves were generated at PZT A and measured at PZT B on the intact target structure. Next, Fig. 5 shows that the measured two signals are changed due to external loads. Based on the observations, both admittance and guided wave signals are changed even when the target structure is not damaged, resulting in false alarms.

To avoid these false alarms, the passive admittance signals are decomposed using Eq. (2). Fig. 6 compares the passive admittance signals. Figs. 6 (a), (b), and (c) show the temperature variation effect, the external loading effect, and structural damage effect on the passive admittance signals, respectively. The passive admittance signals are changed under varying temperature and external loading conditions, while they are not affected by structural damage. Here, although the test results obtained from the fitting lug shown in Fig. 3 (b) are not presented here due to space limitation, the similar patterns can be observed.

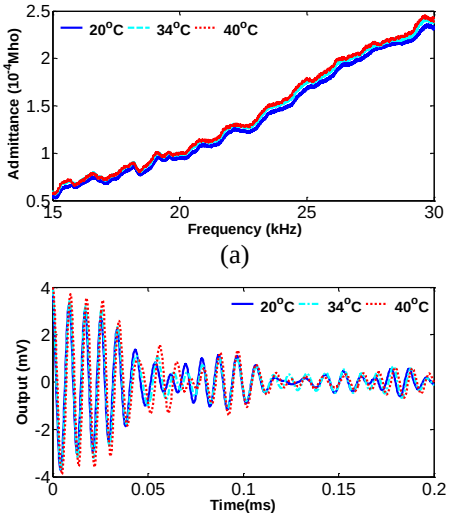

(a)

(b)

Fig. 4. Temperature effects on (a) admittance and (b) guided wave signals obtained from the upper skin of the intact aircraft wing structure

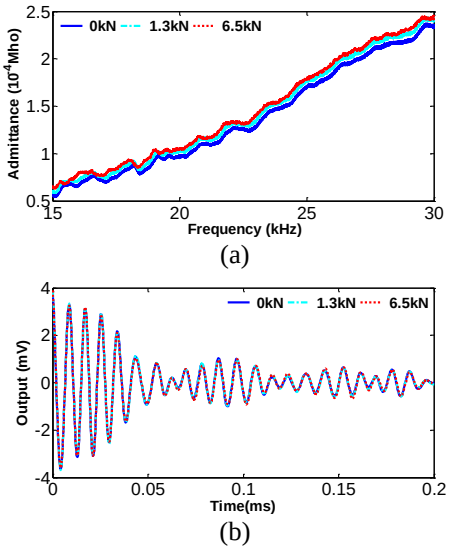

(a)

(b)

Fig. 5. External loading effects on (a) admittance and (b) guided wave signals obtained from the upper skin of the intact aircraft wing structure

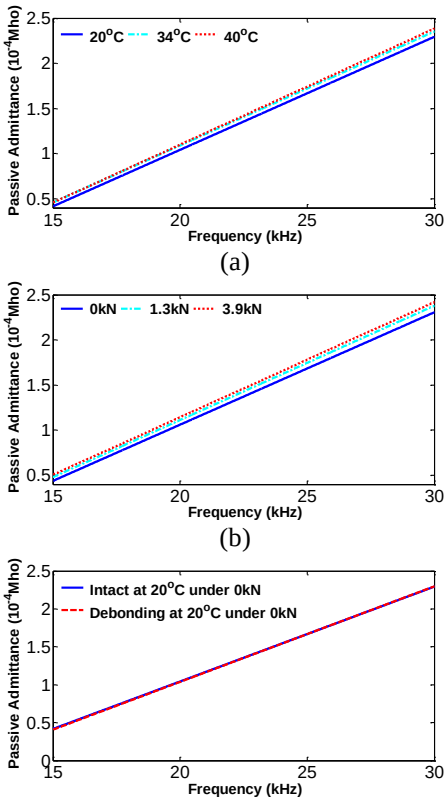

Fig. 6. Comparison of passive admittance signals: (a) Temperature variation effect, (b) External loading effect and (c) Structural damage effect

Table I. Damage Diagnosis Results: Damage is alarmed when DI becomes smaller than TR. Note that the bold values denote the bigger value between TR and DI.

SPOT	CASE	TR	DI	Damage Diagnosis
Upper Skin	Intact	0.9816	**0.9931**	**Intact**
	Debonding	**0.9816**	0.9711	**Damage**
Fitting Lug	Intact	0.6912	**0.7231**	**Intact**
	Bolt loosening	**0.9191**	0.6734	**Damage**

Therefore, environmental variation effects can be minimized using the passive admittance signals. Then DI and TR are computed using the corresponding active admittance and guided wave signals. The damage diagnosis results obtained from the fitting lug as well as the upper skin are summarized in Table I. Here the test data are intentionally obtained from the different environmental conditions. Table I summarizes that there is no false alarm in intact cases while debonding and bolt loosening are successfully detected even under varying temperature as well as external loading condition.

5. Conclusion

This paper presents aircraft wing structure monitoring using integrated impedance and guided wave (IIG) technique. First, IIG measurement system that can simultaneously measure both impedance and guided wave data sets using a single data acquisition system is developed. Second, IIG based damage detection algorithm is proposed. Finally, the applicability of the proposed technique to a full scale aircraft wing structure is examined under varying temperature and external loading conditions. The test results of crack and debonding detection make us possible to confirm the feasibility of the proposed technique. To ensure the performance and reliability of the proposed technique, sufficient amount of baseline data sets, however, should be previously collected and stored under various environmental conditions of the target structure. Further studies are needed so that the IIG based proposed technique is applied to aircraft structures under real operational condition.

References

[1] V. Giurgiutiu, A. Zagrai, J.J. Bao, Piezoelectric wafer embedded active sensors for aging aircraft structural health monitoring, *Structural Health Monitoring* 1 (2002) 41-61.

[2] A. Raghavan, C.E.S. Cesnik, Review of guided-wave structural health monitoring, *Shock Vibration Digest* 39 (2007) 91–114.

[3] V. Giurgiutiu, Structural Health Monitoring with Piezoelectric Wafer Active Sensors. Elsevier, Burlington, MA, 2008.

[4] K. Diamanti, C. Soutis, Structural health monitoring techniques for aircraft composite structures. *Progress in Aerospace Science* 46 (2010) 342–352.

[5] C. Liang, F.P. Sun, C.A. Rogers, Coupled electro-mechanical analysis of adaptive material systems determination of the actuator power consumption and system energy transfer, *Journal of Intelligent Materials and Systems* 5 (1994) 12-20.

[6] S. Bhalla, C.K. Soh, Structural impedance based damage diagnosis by piezo-transducers, *Earthquake Engineering and Structural Dynamics* 32 (2003) 1897-1916.

[7] Y.K. Lin, Probabilistic Theory of Structural Dynamics, McGRAW-Hill, New York, 1967.

[8] S.J. Lee, H. Sohn, Active self-sensing scheme development for structural health monitoring, *Smart Materials and Structures* 15 (2006) 1734-1746.